

Numerical Solution of Boundary Integral Equations for Molecular Electrostatics

Jaydeep P. Bardhan^{1,2}

¹*Mathematics and Computer Science Division,
Argonne National Laboratory, Argonne IL 60439*

²*Department of Physiology and Molecular Biophysics,
Rush University, Chicago IL 60612*

(Dated: March 31, 2008)

Abstract

In this paper we evaluate two approaches to discretizing integral-equation formulations of linear, continuum models for estimating intra- and intermolecular electrostatic interactions in solution. The importance of electrostatic forces in a variety of biological and chemical processes has motivated extensive research into numerical simulation techniques. Boundary-element methods (BEM) represent one popular approach to simulating models based on partial-differential equations (PDEs), and give rise to linear matrix equations. The entries associated with BEM matrices can be calculated in different ways, and in this paper we show that a straightforward approach to discretizing the widely used apparent-surface-charge (ASC) formulation is significantly less accurate than an equivalent but less obvious approach. In contrast, more computationally expensive boundary-integral formulations based on pairs of coupled integral equations exhibit reduced sensitivity to the approach to forming the BEM matrix. We also illustrate the equivalence between the ASC formulation and the double-layer formulation derived by Juffer *et al.*; when their matrix entries are evaluated appropriately, the two formulations produce numerically identical solutions. A similar equivalence exists between the Yoon–Lenhoff and the Bordner–Huber formulations.

1. INTRODUCTION

Electrostatic interactions within and between molecules in solution have long been recognized as playing a variety of important roles in determining molecular structure and binding activity [1], and methods for accurately estimating the strength and character of these interactions have been an active research area for almost as long [2–6]. The complex interactions between solute, solvent molecules, and mobile salt ions pose theoretical and computational modeling challenges for molecular-mechanics-based studies of biomolecules, as well as for *ab initio* quantum-mechanical simulations of small- to medium-sized molecules [5, 7, 8]. Molecular-dynamics (MD) simulations with explicit solvent provide a microscopically detailed picture of solvation, but require computationally expensive sampling of the solvent phase space [9–13]. In contrast, implicit-solvent models sacrifice microscopic detail for computational efficiency [3, 6, 14], and many treat the electrostatic component of the solute–solvent interactions using macroscopic, continuum electrostatic theory [2–4, 6, 6–8, 14–20]. Continuum-theory-based models derive from relatively well-understood second-order elliptic partial-differential equations (PDEs), which represents one reason for their popularity. In addition, there exist well-developed and mature numerical methods for simulating these PDE models, with finite-volume and finite-difference methods (FDMs) [15, 21–31], finite-element methods (FEMs) [26, 32, 33], and boundary-element methods (BEMs) [5, 34–55] among the most common. Generally, models based on continuum theory treat the solvent as a homogeneous medium of high dielectric and the solute as a homogeneous medium of low dielectric, which contains an approximation to the solute charge distribution. Dilute ionic solvents can be modeled using Poisson–Boltzmann theory in either its nonlinear or linearized form [3].

Implicit-solvent models are not a panacea, however. Many types of chemically and biologically important phenomena are modeled poorly or neglected entirely. Continuum models can be exact only in the limit as the size of the solvent molecules approaches zero [56], and their inability to reproduce fine details of the energy surface is well documented (see, for instance, [57, 58]). Furthermore, the Poisson–Boltzmann equation, even in its nonlinear form, ignores mobile ions’ finite size and ion–ion correlations [59–61]. Heterogeneity of the dielectric constant inside the protein may also be important [62]. Despite these limitations, continuum models will likely remain a valuable theoretical tool until alternative models are

developed that can treat these effects at comparable computational expense.

The imperfect nature of these models does, however, warrant the use of accurate numerical methods—computational techniques that generate answers highly faithful to the underlying mathematical model. High-resolution calculations of problems in small-molecule and protein design, for instance, can benefit from well-converged simulations. The ability of numerical methods to obtain converged solutions allows experimental results to be interpreted with respect to the theoretical model used to estimate binding free energies rather than the shortcomings of the employed numerical methods. Self-consistent reaction field (SCRf) treatments of solvent effects in *ab initio* quantum-mechanical simulations represent another area in which well-converged electrostatic simulations are of significant importance [8, 52, 63]. The interpretability of an SCRf-based simulation can depend on whether the solvent treatment may be said to be faithful to the model used.

For implicit-solvent models that treat solute and solvent as regions of homogeneous permittivity, boundary-integral equation formulations offer several attractive theoretical and numerical properties. One advantage is that the dielectric boundaries, which are of primary importance in determining a system’s response to a charge distribution, are represented directly. This focus allows molecular boundaries, which can be highly complex, to be represented accurately [38, 45, 64]. Boundary-integral-equation methods’ explicit focus on solute–solvent boundaries is one reason for their frequent employment in self-consistent reaction field (SCRf) methods that combine *ab initio* electronic-structure methods with a continuum representation of solvent (the literature in this area is extensive; see, e.g., [5, 7, 8, 46, 51, 52, 65, 66]).

Electrostatic integral equations are commonly written using integral operators that can be interpreted as calculating the electrostatic potential or its normal derivative at a dielectric boundary, given a distribution of charge at that boundary. Perhaps the simplest electrostatic-integral equation is the apparent-surface-charge (ASC) formulation presented by Miertus, Scrocco, Tomasi, and collaborators for SCRf calculations (for example, [5, 46, 67]) and later by Shaw, Zauhar, and collaborators for modeling electrostatic interactions in proteins [34–37, 68]. Attard has demonstrated that a variational approach may also be used in its derivation [53]. The ASC formulation is a second-kind Fredholm integral equation [69] whose unknown is a single-layer charge distribution that generates, in the solute region, the same potential as would be generated by polarization of the solvent. The ASC

integral operator maps this distribution of monopole charge on the solute–solvent boundary to the normal electric field at the boundary.

The process by which an infinite-dimensional boundary-integral equation is converted into a finite-dimensional matrix equation is termed *discretization*. In the present paper, we demonstrate that the precise details of the discretization procedure can have a significant impact on simulation accuracy. Our analysis builds on the work of Tausch, Wang, and White, who first noted the inaccurate results obtained from numerical simulations that discretized this electric-field operator using a common BEM technique known as centroid-collocation [70]. By analyzing centroid-collocation as a simplified Galerkin method [69], they were able to identify the source of the inaccuracy and note that the double integrals associated with Galerkin BEM matrices can require a carefully considered combination of analytical and numerical integration. They suggested an alternative approach, *qualocation*, that offered greatly improved accuracy without any increase in computational cost. Qualocation proved to be more accurate than collocation for molecular electrostatic problems also, as demonstrated by Altman *et al.* [71].

In the present work we extend the studies of Tausch *et al.* and Altman *et al.* in two ways. First, the previously employed collocation and qualocation methods represent merely one-point quadrature approximations to the Galerkin double integrals. We therefore investigate the improvement in accuracy as higher-order quadrature rules are employed for numerical integration. Second, previous work has demonstrated only that the ASC formulation is sensitive to the approach to discretization. We assess the sensitivity of the formulations of Yoon and Lenhoff [39], Bordner and Huber [50], and Juffer *et al.* [40] to the different methods for evaluating the Galerkin double integrals.

The following section introduces the key features of the linear continuum electrostatic model under consideration and four boundary-integral-equation formulations of the associated PDE problem. Section 3 describes the boundary-element method for numerically solving boundary-integral equations, focusing on two complementary techniques for calculating the entries of the boundary-element matrices. Section 4 presents the symmetry between the ASC and Juffer double-layer integral equations, as well as one between the Bordner–Huber and Yoon–Lenhoff equations, and demonstrates that the complementary discretizations can preserve these symmetries numerically. Section 5 presents numerical results calculated using the different integral formulations and discretizations. Section 6 concludes the paper.

2. THEORY

2.1. The continuum electrostatic model

Figure 1 is an illustration of the continuum electrostatic model under consideration in this paper. The solute region I is the volume interior to the closed surface Ω , which separates the solvent region II from the solute. Most biomolecule simulations define the solute region using a set of spheres that correspond to atoms or groups of atoms (using a parameter set such as PARSE [72] or that defined by Nina, Im, and Roux [73]), with the boundary Ω defined by rolling a water-molecule-sized probe sphere around the solute spheres [74–76]. In this work, we take the dielectric boundary to be the Richards solvent-excluded surface [75], which is defined as the points of closest approach of the probe-sphere surface to the solute spheres. In *ab initio* self-consistent reaction field (SCRF) calculations, the solute–solvent interface is sometimes defined to be the surface at which the solute electron density falls below a threshold [77, 78].

The electrostatic potential in the solute, $\varphi_I(r)$ is modeled using a Poisson equation

$$\nabla^2\varphi_I(r) = -\rho(r)/\epsilon_I, \tag{1}$$

in which the solute charge distribution is denoted by $\rho(r)$ and the solute dielectric constant is represented by ϵ_I . For most biomolecular simulations, the solute charge distribution $\rho(r)$ is modeled as a set of discrete point charges located at the sphere centers. The solute dielectric constant is typically taken to be between 2 and 8, reflecting electronic polarization and minor structural relaxation [3, 79, 80]. Calculations that treat electronic degrees of freedom explicitly, such as SCRF methods, use a dielectric constant of one in the solute. In the solvent region, the potential $\varphi_{II}(r)$ is modeled as obeying the linearized Poisson–Boltzmann equation

$$\nabla^2\varphi_{II}(r) = \kappa^2\varphi_{II}(r), \tag{2}$$

where κ is the inverse Debye screening length. The solvent is treated as a homogeneous medium with dielectric constant ϵ_{II} , often taken to be 80, approximately that of bulk water. In non-ionic solutions, $\kappa = 0$ and the Laplace equation governs the potential in the solvent.

The electrostatic potential and the normal displacement field are continuous across the interface [81],

$$\varphi_I(r_\Omega) = \varphi_{II}(r_\Omega); \quad (3)$$

$$\epsilon_I \frac{\partial \varphi_I(r_\Omega)}{\partial n(r_\Omega)} = \epsilon_{II} \frac{\partial \varphi_{II}(r_\Omega)}{\partial n(r_\Omega)}, \quad (4)$$

where r_Ω is a point on Ω and $\vec{n}(r_\Omega)$ denotes the outward normal direction at r_Ω pointing from region I into region II . Finally, $\varphi_{II}(r)$ is assumed to obey regularity conditions as $r \rightarrow \infty$ [40].

The solute charge distribution $\rho(r)$ generates a Coulombic potential field and polarizes the solvent, which in turn generates a *reaction potential* $\varphi_{REAC}(r)$ in the solute. The electrostatic potential in region I can therefore be expressed as the sum of the Coulomb potential and the reaction potential induced by solvent polarization:

$$\varphi_I(r) = \varphi_{Coul}(r) + \varphi_{REAC}(r). \quad (5)$$

Calculating $\varphi_{REAC}(r)$ requires solving the coupled system of partial differential equations (PDEs). The difference in electrostatic free energy due to solvent polarization can be written generally as

$$E_{REAC} = \frac{1}{2} \int_{V_I} (\rho(r))^T \varphi_{REAC}(r) d^3r. \quad (6)$$

In the remainder of the paper, it is assumed that the charge distribution $\rho(r)$ is a set of n_c discrete point charges, the i^{th} of which is at r_i and has value q_i :

$$\rho(r) = \sum_{i=1}^{n_c} q_i \delta(r - r_i), \quad (7)$$

where $\delta(r)$ is the Dirac delta function and the n_c -length vector q is the vector of point-charge values. For such charge distributions, (6) reduces to a finite-dimensional inner product of the point-charge values with the reaction potentials induced at the charge locations.

2.2. Boundary-integral equation formulations for molecular electrostatics

The coupled system of partial-differential equations (PDEs) can be reformulated in any of several ways as a system of boundary-integral equations (BIEs). We present the formulations of interest using the notation employed by Chipman [51]. A single-layer (monopole) distribution of charge on the boundary Ω is denoted by $\sigma(r)$, and a double-layer (normally

oriented dipole) distribution by $\mu(r)$. The single-layer potential operator \mathcal{S}_κ , where again κ is the inverse Debye screening length, is defined as

$$\mathcal{S}_\kappa\sigma(r) = \int_{\Omega} \sigma(r')G_\kappa(r; r')d^2r', \quad (8)$$

where $G_\kappa(r; r')$ is the free-space Green's function for the linearized Poisson–Boltzmann equation:

$$G_\kappa(r; r') = \frac{e^{-\kappa\|r-r'\|}}{4\pi\|r-r'\|}. \quad (9)$$

A subscript 0 denotes the non-ionic solvent case in which $\kappa = 0$; thus $G_0(r; r')$ is the free-space Laplace Green's function

$$G_0(r; r') = \frac{1}{4\pi\|r-r'\|}. \quad (10)$$

The single-layer electric-field operator \mathcal{D}_κ^* also acts on $\sigma(r)$ and is defined by

$$\mathcal{D}_\kappa^*\sigma(r) = \int_{\Omega} \sigma(r')\frac{\partial G_\kappa(r; r')}{\partial n(r)}d^2r'. \quad (11)$$

The integral in (11) is improper. In the present paper, every improper integral is assumed to return its principal value; that is, every improper integral is evaluated with an infinitesimally small circular disc around r removed from the domain of integration. The double-layer potential and electric-field operators \mathcal{D}_κ and \mathcal{B}_κ act on the double-layer charge distribution $\mu(r)$ and are defined by

$$\mathcal{D}_\kappa\mu(r) = \int_{\Omega} \mu(r')\frac{\partial G_\kappa(r; r')}{\partial n(r')}d^2r' \quad (12)$$

$$\mathcal{B}_\kappa\mu(r) = \int_{\Omega} \mu(r')\frac{\partial^2 G_\kappa(r; r')}{\partial n(r)\partial n(r')}d^2r'. \quad (13)$$

The integral-equation formulations share a common mathematical structure in which the reaction potential $\varphi_{REAC}(r)$ can be written as the product of three linear operators applied to the solute charge distribution $\rho(r)$:

$$\varphi_{REAC}(r) = M_3M_2^{-1}M_1\rho(r). \quad (14)$$

These operators represent the complete formal description of a particular formulation. The operator M_1 maps the solute charge distribution to a field or set of fields on the boundary Ω ; M_2 maps the unknown surface distributions to the fields to be satisfied on the boundary,

and therefore M_2^{-1} maps from the fields to the unknown surface distributions; and M_3 maps from the surface distributions to the reaction potential in the solute.

Note that the formulations presented below are specialized to the one-boundary problem in Figure 1. Altman *et al.* [82] discuss the implementation of integral-equation methods capable of treating more complex geometries, which may include water-filled cavities in the solute, multiple solutes, and ion-exclusion layers [83].

2.2.1. The Apparent-Surface-Charge (ASC) formulation

Miertus *et al.*, and later Shaw, presented the *apparent-surface-charge* (ASC) integral-equation formulation for biomolecular electrostatics, which is specialized for the case in which $\kappa = 0$:

$$\frac{1}{2} \left(\frac{\epsilon_I + \epsilon_{II}}{\epsilon_I - \epsilon_{II}} \right) \sigma_p(r) + \oint_{\Omega} \left(\frac{\partial G(r; r')}{\partial n(r)} \sigma_p(r') \right) d^2 r' = - \sum_{i=1}^{n_c} \frac{\partial G(r; r_i)}{\partial n(r)} q_i, \quad (15)$$

where $n(r)$, the surface normal at $r \in \Omega$, is defined to point outward from solute into solvent, \oint denotes a principal value integral, and the unknown surface distribution is the single-layer charge density $\sigma_p(r)$ [5, 34]. The reaction potential is calculated from $\sigma_p(r)$ using the relation

$$\varphi_{REAC}(r) = \frac{1}{\epsilon_I} \int_{\Omega} \sigma_p(r') G_0(r; r') d^2 r'. \quad (16)$$

Using Chipman's operator notation, the integral equation (15) can be written as

$$\left(\frac{1}{2} \left(\frac{\epsilon_I + \epsilon_{II}}{\epsilon_I - \epsilon_{II}} \right) I + \mathcal{D}_0^* \right) \sigma_p = -\mathcal{D}_{0, n_c \rightarrow \Omega}^* q, \quad (17)$$

where $\mathcal{D}_{0, n_c \rightarrow \Omega}^*$ maps the n_c point-charge values to the normal component of the electric field at the surface Ω . The reaction potential is written in operator notation as

$$\varphi_{REAC} = \frac{1}{\epsilon_I} \mathcal{S}_{0, \Omega \rightarrow n_c} \sigma_p, \quad (18)$$

and thus the ASC formulation, in the notation of (14), is

$$M_1^{ASC} = -\mathcal{D}_{0, n_c \rightarrow \Omega}^*; \quad (19)$$

$$M_2^{ASC} = \frac{(\epsilon_I + \epsilon_{II})}{2(\epsilon_I - \epsilon_{II})} I + \mathcal{D}_0^*; \quad (20)$$

$$M_3^{ASC} = \frac{1}{\epsilon_I} \mathcal{S}_{0, \Omega \rightarrow n_c}. \quad (21)$$

2.2.2. The Juffer *et al.* (J) formulation and the simplified Juffer *et al.* (SJ) formulation

Juffer *et al.* derived a purely second-kind integral-equation formulation capable of treating the linearized Poisson–Boltzmann problem in the solvent region [40]. The full Juffer (J) formulation consists of a pair of coupled integral equations whose unknowns are a single-layer surface distributions $\sigma(r)$ and a double-layer distribution $\mu(r)$:

$$\begin{bmatrix} \left(\frac{1}{2}(1 + \epsilon_R)I - (\epsilon_R \mathcal{D}_\kappa - \mathcal{D}_0)\right) & (\mathcal{S}_\kappa - \mathcal{S}_0) \\ -(\mathcal{B}_\kappa - \mathcal{B}_0) & \left(\frac{1}{2}(1 + \epsilon_R^{-1})I + (\epsilon_R^{-1} \mathcal{D}_\kappa^* - \mathcal{D}_0^*)\right) \end{bmatrix} \begin{bmatrix} \mu \\ \sigma \end{bmatrix} = \begin{bmatrix} \frac{1}{\epsilon_I} \mathcal{S}_{0,n_c \rightarrow \Omega} \\ \frac{1}{\epsilon_I} \mathcal{D}_{0,n_c \rightarrow \Omega}^* \end{bmatrix} q \quad (22)$$

where $\epsilon_R = \frac{\epsilon_U}{\epsilon_I}$. The Juffer reaction field operator is

$$\varphi_{REAC}(r) = \begin{bmatrix} (\epsilon_R \mathcal{D}_{\kappa, \Omega \rightarrow n_c} \kappa - \mathcal{D}_{0, \Omega \rightarrow n_c}) & (\mathcal{S}_{0, \Omega \rightarrow n_c} - \mathcal{S}_{\kappa, \Omega \rightarrow n_c}) \end{bmatrix} \begin{bmatrix} \mu \\ \sigma \end{bmatrix}. \quad (23)$$

Juffer *et al.* note that when $\kappa = 0$, the formulation can be simplified to an integral-equation with only an unknown dipole-layer distribution $\mu(r)$:

$$\left(\frac{1}{2}(1 + \epsilon_R)I + (1 - \epsilon_R)\mathcal{D}_0\right) \mu = \frac{1}{\epsilon_I} \mathcal{S}_{0,n_c \rightarrow \Omega} q. \quad (24)$$

In the simplified-Juffer (SJ) formulation, the reaction potential is calculated from the dipole distribution by

$$\varphi_{REAC} = (\epsilon_R - 1) \mathcal{D}_{0, \Omega \rightarrow n_c} \mu. \quad (25)$$

2.2.3. The Bordner–Huber (BH) formulation

Bordner and Huber derived a pair of coupled integral equations whose unknowns are two single-layer distributions, one interior and one exterior to Ω [50]. Denoting the interior distribution by σ_i and the exterior by σ_e , the integral equations are

$$\begin{bmatrix} -\frac{\epsilon_I}{\epsilon_{II}} \left(\frac{1}{2}I + \mathcal{D}_0^*\right) & -\frac{1}{2}I + \mathcal{D}_\kappa^* \\ -\mathcal{S}_0 & \mathcal{S}_\kappa \end{bmatrix} \begin{bmatrix} \sigma_i \\ \sigma_e \end{bmatrix} = \begin{bmatrix} \frac{1}{\epsilon_{II}} \mathcal{D}_{0,n_c \rightarrow \Omega}^* \\ \frac{1}{\epsilon_I} \mathcal{S}_{0,n_c \rightarrow \Omega} \end{bmatrix} q. \quad (26)$$

The reaction potential can be calculated from $\sigma_i(r)$ by the relation

$$\varphi_{REAC} = \mathcal{S}_{0, \Omega \rightarrow n_c} \sigma_i. \quad (27)$$

2.2.4. The Yoon–Lenhoff (YL) formulation

Yoon and Lenhoff derived a formulation whose unknowns are the electrostatic potential $\varphi(r)$ and its normal derivative just inside the boundary, $\frac{\partial\varphi(r)}{\partial n(r)}$. These quantities satisfy the coupled equations

$$\begin{bmatrix} \frac{1}{2}I + \mathcal{D}_0 & -\mathcal{S}_0 \\ \frac{1}{2}I - \mathcal{D}_\kappa & \frac{\epsilon_I}{\epsilon_{II}}\mathcal{S}_\kappa \end{bmatrix} \begin{bmatrix} \varphi \\ \frac{\partial\varphi}{\partial n} \end{bmatrix} = \begin{bmatrix} \frac{1}{\epsilon_I}\mathcal{S}_{0,n_c \rightarrow \Omega} \\ 0 \end{bmatrix} q, \quad (28)$$

and the reaction potential at the charge locations is

$$\varphi_{REAC} = \begin{bmatrix} -\mathcal{D}_{0,\Omega \rightarrow n_c} & +\mathcal{S}_{0,\Omega \rightarrow n_c} \end{bmatrix} \begin{bmatrix} \varphi \\ \frac{\partial\varphi}{\partial n} \end{bmatrix}. \quad (29)$$

3. NUMERICAL DISCRETIZATION OF BOUNDARY INTEGRAL EQUATIONS USING BOUNDARY-ELEMENT METHODS

An electrostatic capacitance calculation provides a simple example for presenting the boundary-element method. Consider a perfectly conducting sphere of 1-meter radius suspended in free space. Its capacitance is equal to the ratio of the total charge induced on its surface when the sphere is raised to a 1 Volt potential relative to ground. The capacitance of the sphere can be calculated by solving the integral equation

$$\psi(r) = \int_{\Omega} K(r; r')\sigma(r')d^2r', \quad (30)$$

where the surface potential $\psi(r) = 1$ Volt, Ω is the sphere boundary, $\sigma(r)$ is the unknown charge distribution, and the kernel $K(r; r')$ is the free-space Laplace Green's function $G_0(r; r')$. Boundary-integral equations such as (30) can be solved numerically using the boundary-element method (BEM) [69]. In BEM, one first introduces a set of n_e linearly independent *basis functions* $\chi_1(r), \chi_2(r), \dots, \chi_{n_e}(r)$ defined on the boundary of interest, or on an approximation to it. The extension to formulations with multiple unknown surface distributions is straightforward. The space of approximate solutions is the set of weighted combinations of these basis functions, so that any member of this set can be written as

$$\hat{\sigma}(r) = \sum_{i=1}^{n_e} x_i \chi_i(r), \quad (31)$$

where x_i represents the weight for the i^{th} basis function. In general, the finite-dimensional basis does not allow the integral equation (30) to be satisfied at all points on the boundary

or boundary approximation. It is therefore of interest to find an approximate solution that matches the true solution as closely as possible, and the usual approach is to force the residual

$$R(r) = f(r) - \int_{\Omega} \left(K(r; r') \sum_{i=1}^{n_e} x_i \chi_i(r) \right) d^2 r' \quad (32)$$

to be orthogonal to a set of *test functions* defined on Ω . Denoting the j^{th} of N test functions by $\gamma_j(r)$, the corresponding constraint on the residual is

$$\int_{\Omega} \gamma_j(r) \left[f(r) - \int_{\Omega} \left(K(r; r') \sum_{i=1}^N x_i \chi_i(r) \right) d^2 r' \right] d^2 r = 0. \quad (33)$$

Using N basis functions to represent the unknown distribution and forcing the residual to be orthogonal to each of N test functions produces a square matrix equation

$$Ax = b, \quad (34)$$

where each matrix entry is defined according to

$$A_{ij} = \int_{\Omega} \left[\gamma_i(r) \int_{\Omega} (K(r; r') \chi_j(r')) d^2 r' \right] d^2 r \quad (35)$$

and b_i , the i^{th} entry of the right hand side, is

$$b_i = \int_{\Omega} \gamma_i(r) f(r) d^2 r. \quad (36)$$

3.1. Basis Functions and Boundary Discretization

For many problems with complex geometries, it is impractical or impossible to determine, *a priori*, a basis set that is sufficiently complete to ensure accurate solution of the integral equation, and yet as small as possible to minimize simulation time. The boundaries of interest are therefore commonly discretized into subdomains, or *boundary elements*, for which basis functions can be defined more easily. Many BEM simulations are performed with boundary elements that approximate the original boundaries using planar triangles, planar quadrilaterals, or quadratic boundary elements [37, 41, 84–87]. In some special cases, boundary elements can be used that can exactly describe the boundaries under consideration (see, for example, [38, 45, 64]). In this paper, we approximate the solute–solvent interfaces using planar triangles and introduce piecewise-constant basis functions defined by

$$\chi_i(r) = \begin{cases} 1 & \text{if } r \text{ is on boundary element } i \\ 0 & \text{otherwise.} \end{cases} \quad (37)$$

These boundary-element representations are termed boundary discretizations.

3.2. Test Functions

Boundary-element simulations frequently employ one of two types of test functions. The first consist of delta functions and therefore force the integral equation to be satisfied exactly at specified locations. These approaches are commonly described as *point-collocation* boundary-element methods. Centroid-collocation methods, for instance, force the integral equation to be exactly satisfied at the centroid of each boundary element. Defining r_{c_i} to be the centroid of the i^{th} boundary element, the matrix entries of (34) are

$$A_{ij} = \int_{\Omega_j} \chi_j(r') K(r_{c_i}; r') d^2 r', \quad (38)$$

where Ω_j represents the support of the j^{th} basis function; for piecewise-constant basis functions defined by (37), Ω_j is the j^{th} boundary element. The right-hand side is defined by

$$b_i = f(r_{c_i}). \quad (39)$$

When the set of test functions is the same as the set of basis functions, one obtains what are known as *Galerkin* BEM techniques. The matrix entries in such methods are

$$A_{ij} = \int_{\Omega_i} \chi_i(r) \int_{\Omega_j} \chi_j(r') K(r; r') d^2 r' d^2 r. \quad (40)$$

3.3. Evaluating Galerkin Double Integrals

For the piecewise-constant basis functions used in this work, the Galerkin double integrals A_{ij} in (40) are readily interpreted as the integral, over element i , of the potential (or normal electric field) induced by the uniform charge distribution $\chi_j(r)$. Analytical methods for computing Galerkin double integrals of the form (40) exist only for specialized geometries and kernels [88]. Numerical quadrature [89] must therefore be used to evaluate at least one of the integrals in (40). Numerical quadrature methods usually approximate the integral of a function $f(x)$ over a domain D as

$$\int_D f(x) dx \approx \sum_{i=1}^{n_p} w_i f(x_i), \quad (41)$$

where n_p represents the number of points used in approximating the integral, x_i is the i^{th} quadrature point, and w_i is the corresponding weight. Integrals of smoothly varying functions such as polynomials can often be approximated to very high accuracy using relatively few quadrature points. For example, in one dimension a n_p -point Gauss quadrature rule exactly integrates polynomials up to degree $2n_p - 1$. In contrast, discontinuous or sharply peaked functions can require many quadrature points to achieve a desired accuracy.

Analytical techniques do exist for computing the Coulomb potential and its gradient at any single point in space, given a polynomially-varying distribution of single- or double-layer charge on a planar, polygonal boundary element [88, 90, 91]. It is therefore natural to evaluate the integrals in the order in which they appear in (40). The outer integral over Ω_i is approximated using numerical quadrature, and the inner integral is evaluated repeatedly. The matrix entries then take the form

$$A_{ij} = \sum_{k=1}^{n_p} w_k^{(i)} \gamma_i(r_k^{(i)}) \int_{\Omega_j} \chi_j(r') K(r_k^{(i)}; r') d^2 r', \quad (42)$$

where n_p is the order of the quadrature rule and $w_k^{(i)}$ and $r_k^{(i)}$ represent the weight and location of the k^{th} quadrature point on element i . In this paper, this approach to evaluating the matrix entries is termed a n_p -point *basis-inner* discretization. In the special case $n_p = 1$, the point $r_k^{(i)}$ is necessarily the panel centroid, and the weight $w_k^{(i)}$ is the panel area. Thus, the BEM matrix generated by a centroid-collocation method is the same as that produced by a one-point basis-inner Galerkin method, subject to a row scaling [70].

For the electrostatic kernels described in this paper, the order of integration in (40) can be reversed [69, 70]. In this paper, such an approach is called a *test-inner* discretization because the integral over the test function's support that is evaluated first and the integration over the basis-function support is evaluated numerically. This technique generates matrix entries of the form:

$$A_{ij} = \sum_{k=1}^{n_p} w_k^{(j)} \chi_j(r_k^{(j)}) \int_{\Omega_i} \gamma_i(r) K(r; r_k^{(j)}) d^2 r. \quad (43)$$

Using a one-point quadrature rule to evaluate (43), one obtains what Tausch, Wang, and White termed a *quallocation* method [70]:

$$A_{ij} = \alpha_j \chi_j(r_{c_j}) \int_{\Omega_i} \gamma_i(r) K(r; r_{c_j}) d^2 r, \quad (44)$$

where α_j is the area of panel j . For a fixed quadrature order n_p , the cost to evaluate a particular matrix entry is essentially independent of whether (42) or (43) is used.

Galerkin boundary-element integrals associated with the LPBE Green’s function can be evaluated by using the techniques described above to calculate the Poisson Galerkin double integrals and then adding the correction term described by Boschitsch *et al* [49].

4. DUALITY RELATIONSHIPS BETWEEN INTEGRAL-EQUATION FORMULATIONS

Section 2 presented several integral-equation formulations for molecular electrostatics, including the Bordner–Huber (BH) formulation, the Yoon–Lenhoff (YL) formulation, the apparent-surface-charge (ASC) formulation, and the simplified-Juffer (SJ) formulation. In this section, we derive one symmetry relation between the ASC and SJ formulations and another between the BH and YL formulations. In addition, we demonstrate that the complementary test-inner and basis-inner discretizations described in the previous section preserve these symmetries during numerical simulation. The existence of these symmetries indicates that differences in accuracy between the equivalent formulations reflects the discretizations employed rather than inherent advantages of one formulation relative to the other.

4.1. Duality of the Apparent-Surface-Charge and Simplified-Juffer Formulations

Clearly, multiplying M_1^{ASC} and M_2^{ASC} by the quantity $(1 - \epsilon_R)$ preserves the original solution σ_p , and we can therefore use the modified operators

$$\hat{M}_1^{ASC} = (\epsilon_R - 1) \mathcal{D}_{0,n_c \rightarrow \Omega}^*; \tag{45}$$

$$\hat{M}_2^{ASC} = \left(\frac{1}{2} (1 + \epsilon_R) I + (1 - \epsilon_R) \mathcal{D}_0^* \right), \tag{46}$$

to write the ASC reaction potential as

$$\varphi_{REAC} = M_3^{ASC} \hat{M}_2^{ASC, -1} \hat{M}_1^{ASC} q. \tag{47}$$

Comparing the re-scaled ASC operators to those of the simplified-Juffer formulation in (24), it is clear that \hat{M}_1^{ASC} is the transpose of the SJ operator M_3^{SJ} ; similarly, $\hat{M}_2^{ASC} = M_2^{SJ,T}$ and $M_3^{ASC} = M_1^{SJ,T}$.

This symmetry can be preserved numerically using the complementary test-inner and basis-inner approaches presented in Section 3.3. If analytical integration techniques [90, 91]

are used to evaluate the inner integrals, the matrix entries for the corresponding operators are exactly equal. A test-inner method with a quadrature rule of order n_p for the ASC formulation generates matrix entries of the form

$$\hat{M}_{1,ij}^{ASC} = (\epsilon_R - 1) \int_{\Omega_i} \frac{\partial G_0(r; r_j)}{\partial n(r)} d^2 r; \quad (48)$$

$$\hat{M}_{2,ij}^{ASC} = \sum_{k=1}^{n_p} w_k^{(j)} \chi_j(r_k^{(j)}) \int_{\Omega_i} \chi_i(r) \frac{\partial G_0(r; r_k^{(j)})}{\partial n(r)} d^2 r; \quad (49)$$

$$M_{3,ij}^{ASC} = \frac{1}{\epsilon_I} \int_{\Omega_j} G_0(r_i; r) d^2 r. \quad (50)$$

A basis-inner discretization of equal order for the SJ formulation generates matrices with entries

$$M_{1,ij}^{SJ} = \frac{1}{\epsilon_I} \int_{\Omega_i} G_0(r; r_j) d^2 r; \quad (51)$$

$$M_{2,ij}^{SJ} = \sum_{k=1}^{n_p} w_k^{(i)} \chi_i(r_k^{(i)}) \int_{\Omega_j} \chi_j(r) \frac{\partial G_0(r_k^{(i)}; r)}{\partial n(r)} d^2 r; \quad (52)$$

$$M_{3,ij}^{SJ} = (\epsilon_R - 1) \int_{\Omega_j} \frac{\partial G_0(r_i; r)}{\partial n(r)} d^2 r. \quad (53)$$

The analogous result holds when the basis-inner discretization is used for the ASC formulation and the test-inner method is used for the SJ formulation.

4.2. Duality of the Bordner–Huber and Yoon–Lenhoff Formulations

The Bordner–Huber (BH) and Yoon–Lenhoff (YL) formulations also share a symmetry relationship under simple scaling transformations. Multiplying both M_1^{BH} and M_2^{BH} on the left by

$$\begin{bmatrix} -\epsilon_{II} I & \\ & \epsilon_I I \end{bmatrix} \quad (54)$$

and right-multiplying both M_2^{BH} and M_3^{BH} by

$$\begin{bmatrix} \frac{1}{\epsilon_I} I & \\ & \frac{1}{\epsilon_{II}} I \end{bmatrix} \quad (55)$$

produces the modified matrices

$$\hat{M}_1^{BH} = \begin{bmatrix} -\mathcal{D}_0^* \\ \mathcal{S}_0 \end{bmatrix}; \quad (56)$$

$$\hat{M}_2^{BH} = \begin{bmatrix} (\frac{1}{2}I + \mathcal{D}_0^*) & (\frac{1}{2}I - \mathcal{D}_\kappa^*) \\ -\mathcal{S}_0 & \frac{\epsilon_I}{\epsilon_{II}}\mathcal{S}_\kappa \end{bmatrix}; \quad (57)$$

$$\hat{M}_3^{BH} = \begin{bmatrix} \frac{1}{\epsilon_I}\mathcal{S}_0 & 0 \end{bmatrix}, \quad (58)$$

and then clearly $M_3^{BH,T} = M_1^{YL}$, $M_2^{BH,T} = M_2^{YL}$, and $M_1^{BH,T} = M_3^{YL}$. An analysis similar to that of Section 4.1 shows that discretizing the BH formulation with either the test- or basis-inner method, and discretizing the YL formulation with the other method, generates numerically identical matrices.

5. COMPUTATIONAL RESULTS

The integral formulations discussed in Section 2 have been used to solve several test cases numerically. For all simulations, planar-triangle boundary elements were used to approximate the solute–solvent interfaces, which were taken to be the Richards solvent-excluded surface [75, 76]. Piecewise-constant basis functions were used to approximate the surface distributions. The solute dielectric constant was taken to be $\epsilon_I = 4$, and the solvent dielectric constant $\epsilon_{II} = 80$. For simulations in which the LPBE was assumed to hold in the solvent region, the inverse Debye screening length κ was taken to be 0.125 \AA^{-1} . The program MSMS [92] was used to generate discretizations of the solute–solvent interfaces using PARSE radii [72] and a probe radius of 1.4 \AA . The boundary-element simulations were conducted using software derived from the FFTSVD fast-solver library [71, 82, 93]. The simulations reported in this work did not utilize the FFTSVD matrix sparsification algorithm or others such as fast multipole [94, 95] or precorrected-FFT [96, 97]. The linear systems were formed explicitly and solved using either the SVD or GMRES [98]. Evaluation of the electrostatic potential due to constant-density single-layer and double-layer charge distributions over planar triangles was accomplished using analytic integration methods [90, 91]. The LPBE integrals were calculated using the desingularization method described by Boschitsch *et al.* [49]. For systems solved using GMRES, no restarts were allowed and iteration was terminated at a tolerance of 10^{-10} relative to the initial preconditioned residual. For the

ASC and SJ formulations, diagonal preconditioners were employed, with $P_{ii} = (M_2^{ii})^{-1}$. For the BH, YL, and J formulations, block preconditioners were used [82, 99]. Quadrature rules presented by Stroud [89] were used to evaluate the outer integrals associated with the Galerkin basis-inner and test-inner discretizations.

5.1. Sphere with Central Charge in Non-Ionic Solution

The implementations of the integral-equation formulations were verified by calculating the electrostatic solvation free energy of a 1 Å-radius sphere with a centrally located unit +1 e charge; the surface was triangulated using vertex densities varying from 1 Å⁻² to 28 Å⁻². This simple geometry has an analytical solution in the case when $\kappa = 0$ and a closed-form solution in the case when $\kappa = 0.125$ Å⁻¹ [39]. Figure 2 is a plot of the absolute errors when $\kappa = 0$ for the apparent-surface-charge and the simplified Juffer *et al.* formulations, discretized using basis-inner and test-inner Galerkin methods. As expected from the analysis in Section 4.1, the basis-inner ASC results are identical to those of the test-inner simplified Juffer method, and similarly the test-inner ASC results are equal to those of the basis-inner simplified-Juffer method. Having demonstrated the equivalence between these two formulations, in the remainder of the paper we denote these formulations collectively as the ASC/SJ formulation. Comparisons between discretizations are drawn only between the test-inner ASC and basis-inner ASC method.

The discrepancy in solution accuracy between the test-inner and basis-inner methods results directly from the smoothness of the functions that are integrated numerically in (42) and (43) [70]. Tausch *et al.* originally explained the inadequacy of numerical quadrature for evaluating the outer integrals associated with centroid-collocation-like basis-inner discretizations like (42) when $K(r; r') = \frac{\partial G(r; r')}{\partial n(r)}$ and boundary elements i and j are adjacent planar boundary elements that share a common edge but have different surface normals. The normal electric field on element i due to a uniform distribution of single-layer charge on element j is sharply peaked close to the edge. Consequently, one-point quadrature methods, like centroid-collocation, poorly approximate the needed integral. The SJ-test-inner and ASC-basis-inner answers therefore change significantly and exhibit improved accuracy with increasing quadrature order.

In contrast, the test-inner approach to evaluating the Galerkin double integrals can be

interpreted as using numerical quadrature to integrate, over element j , the potential induced by a normally oriented dipole distribution on element i . This potential is smooth everywhere over element j and therefore low-order quadrature suffices (see Figure 1 in [70]); the SJ-basis-inner and ASC-test-inner results are essentially the same for all quadrature rules (Figure 2). This supports the use by Tausch *et al.* of only a one-point quadrature rule. The one-point test-inner discretization of the ASC formulation actually offers better accuracy than basis-inner discretizations with higher-order quadrature, and conversely the basis-inner discretization offers superior accuracy for the SJ formulation.

The absolute errors from simulations based on the Yoon and Lenhoff formulation and the Bordner and Huber formulation are plotted in Figure 3(a). The test-inner and the basis-inner results confirm the analysis of Section 4.2; accordingly, in the remainder of the paper these formulations are referred to as the BH/YL formulation generally, and as one or the other when specifying a particular discretization. The coupled formulations exhibit reduced sensitivity compared to the ASC and SJ formulations, because the electric-field operator \mathcal{D}_κ^* of the BH formulation (equivalently, the dipole-layer potential operator \mathcal{D}_κ of the YL formulation) is not the only operator in the integral formulation, and furthermore decays more quickly than the single-layer potential kernel \mathcal{S}_κ .

The results in Figure 3(a) seem contrary to the results of Figure 2, suggesting that better accuracy is obtained when the electric-field operator is discretized using a basis-inner approach. The comparison to the analytical solution is misleading; which discretization provides better accuracy, relative to the analytical result, depends on whether the interior or exterior dielectric constant is larger (data not shown). Because the computed matrix entries are numerical approximations to the the Galerkin double integrals (40), the appropriate baseline for comparison is a Galerkin method in which numerical quadrature has been performed with high precision. In such a comparison only one detail, the manner of imposing the Galerkin orthogonality constraints, is varied between the calculated reference energy and the calculations of interest. Plotted in Figure 3(b) are the deviations of electrostatic free energies calculated using different quadrature rules compared to those calculated using the same discretization method and 18-point quadrature. For each boundary-element representation of the sphere surface, test-inner discretizations of the electric-field operator (and therefore basis-inner discretizations of the double-layer potential operator) generate answers that agree closely regardless of the number of quadrature points used. The alter-

native methods deviate substantially if low-order quadrature is used and converge as the number of quadrature points is increased.

5.2. Formamide

The small molecule formamide was also simulated. Because no analytically determined molecular electrostatic free energy is available, a much more computationally demanding and accurate boundary-integral method, based on curved boundary elements, was used as a reference calculation [64, 82]. Figure 4(a) and (b) are plots illustrating the accuracy associated with different discretization methods when simulating the non-ionic ASC/SJ formulation as well as the BH/YL and J formulations with $\kappa = 0.0$. In Figure 5(a), (b), and (c) are plots of the preconditioned and unpreconditioned GMRES residuals at each iteration using the different formulations and approaches to evaluating the Galerkin double integrals. These convergence plots were obtained using a 1600-element discretization of the formamide molecular surface. The similar GMRES convergence behavior for the basis-inner and test-inner methods indicates that the methods generate matrices of similar conditioning; the singular value decomposition was then used to confirm that the approach to calculating the Galerkin double integrals does not appreciably impact the condition number associated with the BEM matrix (data not shown).

The impact of the electric-field operator discretization approach was assessed for the multi-operator BH/YL, and J formulations by using basis-inner discretization for the single-layer operator \mathcal{S}_0 and varying the discretization employed for the double-layer potential operator \mathcal{D}_0 and the electric-field operator \mathcal{D}_0^* . Figure 6(a) and (b) contains four convergence plots for the J formulation: basis-inner-only, basis-inner with test-inner for \mathcal{D}_0 only, basis-inner with test-inner for \mathcal{D}_0^* only, and basis-inner with test-inner for both \mathcal{D}_0 and \mathcal{D}_0^* . Figure 6(c) illustrates deviations from the curved-element reference calculation for the BH formulation using basis-inner-only and a mixed basis-inner/test-inner method. It is clear that accuracy depends on using an appropriate method to approximate the double integrals corresponding to the normal electric field kernel and dipole-potential kernel. In Figure 6(a) the accuracy does not seem to depend strongly on the method used to discretize the electric-field operator \mathcal{D}_0^* . This phenomenon results from the relative scaling of the diagonal blocks of the formulation (22).

5.3. Peptide

To assess the impact of discretization on simulations of larger biomolecules, a 32-residue α -helix from Lavigne *et al.* [100] was simulated, using atomic coordinates provided by Feig *et al.* [101]. Reference calculations were again performed using high-accuracy, curved-element methods [82]. The deviations from these calculations are shown in Figure 7. The 1-point test-inner and basis-inner discretizations of the ASC formulation again produce answers that differ significantly. Higher-order quadrature does not appreciably improve the accuracy of the ASC/test-inner method but it does improve the accuracy of the ASC/basis-inner method. Relatively small differences are observed between the basis-inner and test-inner discretizations of the BH/YL formulation, and the deviations relative to the reference calculation change appreciably as the number of quadrature points is increased.

6. SUMMARY

The present paper has presented two approaches to discretizing boundary-integral equation formulations of linear, continuum models of solute–solvent electrostatic interactions. It has been seen that the electric-field operator and the double-layer potential operator require appropriate discretization to preserve solution accuracy. By using higher-order numerical quadrature and by implementing the basis-inner and test-inner approaches for several integral-equation formulations, we have extended the analyses of Tausch *et al.* [70] and Altman *et al.* [71]. The Galerkin-method analysis presented by Tausch *et al.* should hold for curved-element methods and higher-order basis functions so long as the boundary-element normals are discontinuous across element boundaries [70]. An investigation of discretization methods for higher-order boundary elements [45] and basis functions [39] is warranted, and represents one area of current research. Further discretization studies also may help to explain why the accuracy of the BH/YL formulation can degrade as the number of quadrature points is increased (Figure 7(b)). One possible explanation is that higher-order quadrature rules magnify the effect of the boundary-discretization error introduced by approximating the molecular surface using planar triangles. A related topic for future work would be to compare the accuracy of simulations that model the apparent-surface-charge layer using discrete point charges to the accuracy of those employ charge-density basis functions.

The numerical results in Section 5 indicate that when the appropriate discretization method is employed, quadrature rules using more than one point offer surprisingly little improvement in accuracy relative to the increase in computational effort. For boundary-element problems solved using dense-matrix GMRES, as well as for sufficiently small problems solved using matrix factorization, the explicit calculation of the boundary-element matrix can represent a substantial fraction of the total computational cost. Because the cost to form the BEM matrix scales linearly in the number of quadrature points, low-order quadrature in conjunction with the appropriate discretization technique can offer both accuracy and performance advantages relative to higher-order quadrature schemes, depending on the discretization. The techniques discussed in this paper may be particularly relevant for boundary-element-based self-consistent reaction-field calculations in which accuracy is often of primary importance.

We have also described the symmetry relationships between two pairs of integral formulations. The apparent-surface-charge formulation is equivalent, in a Galerkin sense, to the simplified Juffer *et al.* formulation. Discretizing one formulation using a test-inner method and the other with an equal-order basis-inner method can produce numerically identical matrices and therefore equal electrostatic free energies. The Yoon–Lenhoff and Bordner–Huber formulations share a similarly symmetric relationship. Because all of these approaches ultimately yield the same reaction potential, it seems manifest that the formulations should be intimately connected. However, the explicit symmetries discussed in Section 4 do not appear to have been noted previously.

Juffer *et al.* observed the difference in accuracy between their double-layer charge formulation (here termed the SJ formulation) and the ASC formulation [40]. In that work, the discrepancy was attributed to the need for the ASC method to match the sharply peaked normal electric field at the boundary, compared to the smoother potential condition matched in the SJ method [40]. Although it is true that the normal electric field is more sharply peaked, the analysis in Section 4 indicates that the discrepancy should be attributed to the Galerkin-approximation characteristics of the collocation method employed there, rather than to the representation of the surface-charge density in the discretized ASC formulation. Finally, it is worth emphasizing that all of the discretizations generate matrices of similar condition number. It is well-known that purely second-kind formulations exhibit significantly better conditioning relative to other formulations [45, 69]. However, the analysis

and computational results presented here illustrate that matrix conditioning alone does not guarantee accuracy with respect to the free energies of interest. Furthermore, it is clear that demonstrations of a technique's convergence do not preclude the existence of techniques with improved accuracy.

7. ACKNOWLEDGMENTS

The author is indebted to M. Anitescu, M. Radhakrishnan, and R. S. Eisenberg for useful discussions, and gratefully acknowledges funding from a Wilkinson Fellowship in Scientific Computing funded by the Mathematical, Information, and Computational Sciences Division Subprogram of the Office of Advanced Scientific Computing Research, Office of Science, U. S. Dept. of Energy, under Contract DE-AC02-06CH11357. The author is also grateful to the Radon Institute for Computational and Applied Mathematics at Johannes Kepler Universität, Linz Austria, for its hospitality and support while much of this work was conducted.

-
- [1] J. G. Kirkwood. Theory of solutions of molecules containing widely separated charges with special application to zwitterions. *Journal of Chemical Physics*, 2:351, 1934.
 - [2] C. Tanford and J. G. Kirkwood. Theory of protein titration curves I. General equations for impenetrable spheres. *Journal of the American Chemical Society*, 59:5333–5339, 1957.
 - [3] K. A. Sharp and B. Honig. Electrostatic interactions in macromolecules: Theory and applications. *Annual Review of Biophysics and Biophysical Chemistry*, 19:301–332, 1990.
 - [4] B. Honig and A. Nicholls. Classical electrostatics in biology and chemistry. *Science*, 268:1144–1149, 1995.
 - [5] S. Miertus, E. Scrocco, and J. Tomasi. Electrostatic interactions of a solute with a continuum – a direct utilization of *ab initio* molecular potentials for the prevision of solvent effects. *Chemical Physics*, 55(1):117–129, 1981.
 - [6] J. Warwicker and H. C. Watson. Calculation of the electric potential in the active site cleft due to alpha-helix dipoles. *Journal of Molecular Biology*, 157:671–679, 1982.
 - [7] M. Orozco and F. J. Luque. Theoretical methods for the description of the solvent effect in biomolecular systems. *Chemical Reviews*, 100:4187–4225, 2000.

- [8] C. J. Cramer and D. G. Truhlar. Implicit solvation models: Equilibria, structure, spectra, and dynamics. *Chemical Reviews*, 99:2161–2200, 1999.
- [9] V. Lounnas, B. M. Pettitt, L. Findsen, and S. Subramaniam. A microscopic view of protein solvation. *Journal of Physical Chemistry*, 18:7157–7159, 1992.
- [10] J. A. McCammon and S. C. Harvey. *Dynamics of Proteins and Nucleic Acids*. Cambridge University Press, Cambridge, 1987.
- [11] C. L. Brooks, III, M. Karplus, and B. M. Pettitt. Proteins: A theoretical perspective of dynamics, structure and thermodynamics. *Adv. Chem. Phys.*, 71:1–249, 1988.
- [12] A. Jean-Charles, A. Nicholls, K. Sharp, B. Honig, A. Tempczyk, T. F. Hendrickson, and W. C. Still. Electrostatic contributions to solvation energies: Comparison of free energy perturbation and continuum calculations. *Journal of the American Chemical Society*, 113:1454–1455, 1991.
- [13] S. W. Rick and B. J. Berne. The aqueous solvation of water: A comparison of continuum methods with molecular dynamics. *Journal of the American Chemical Society*, 116:3949–3954, 1994.
- [14] B. Roux and T. Simonson. Implicit solvent models. *Biophysical Chemistry*, 78:1–20, 1999.
- [15] M. K. Gilson, A. Rashin, R. Fine, and B. Honig. On the calculation of electrostatic interactions in proteins. *Journal of Molecular Biology*, 183:503–516, 1985.
- [16] M. E. Davis and J. A. McCammon. Electrostatics in biomolecular structure and dynamics. *Chemical Reviews*, 90:509–521, 1990.
- [17] B. Honig, K. Sharp, and A. S. Yang. Macroscopic models of aqueous solutions: Biological and chemical applications. *Journal of Physical Chemistry*, 97(6):1101–1109, 1993.
- [18] J. A. Grant, B. T. Pickup, and A. Nicholls. A smooth permittivity function for Poisson-Boltzmann solvation methods. *Journal of Computational Chemistry*, 22:608–640, 2001.
- [19] J. A. Wagoner and N. A. Baker. Assessing implicit models for nonpolar mean solvation forces: The importance of dispersion and volume terms. *Proceedings of the National Academy of Sciences of the USA*, 103(22):8331–8336, 2006.
- [20] J. Wagoner and N. A. Baker. Solvation forces on biomolecular structures: A comparison of explicit solvent and Poisson-Boltzmann models. *J. Comp. Chem.*, 25:1623–1629, 2004.
- [21] M. K. Gilson and B. Honig. Calculation of the total electrostatic energy of a macromolecular system: Solvation energies, binding energies, and conformational analysis. *Proteins*:

- Structure, Function, Genetics*, 4:7–18, 1988.
- [22] M. K. Gilson, K. A. Sharp, and B. H. Honig. Calculating the electrostatic potential of molecules in solution: Method and error assessment. *Journal of Computational Chemistry*, 9:327–335, 1988.
- [23] A. Nicholls and B. Honig. A rapid finite difference algorithm, utilizing successive over-relaxation to solve the Poisson–Boltzmann equation. *Journal of Computational Chemistry*, 12:435–445, 1991.
- [24] M. Holst and F. Saied. Multigrid solution of the Poisson–Boltzmann equation. *Journal of Computational Chemistry*, 14:105–113, 1993.
- [25] J. D. Madura, J. M. Briggs, R. C. Wade, M. E. Davis, B. A. Luty, A. Ilin, J. Antosiewicz, M. K. Gilson, B. Bagheri, L. Ridgway-Scott, and J. A. McCammon. Electrostatics and diffusion of molecules in solution: Simulations with the University of Houston Brownian Dynamics program. *Computer Physics Communications*, 91:57–95, 1995.
- [26] M. Holst, N. Baker, and F. Wang. Adaptive multilevel finite element solution of the Poisson–Boltzmann equation I. Algorithms and examples. *Journal of Computational Chemistry*, 21:1319–1342, 2000.
- [27] W. Rocchia, E. Alexov, and B. Honig. Extending the applicability of the nonlinear Poisson–Boltzmann equation: Multiple dielectric constants and multivalent ions. *Journal of Physical Chemistry B*, 105:6507–6514, 2001.
- [28] N. A. Baker, D. Sept, M. J. Holst, and J. A. McCammon. Electrostatics of nanoystems: Application to microtubules and the ribosome. *Proceedings of the National Academy of Sciences of the USA*, 98:10037–10041, 2001.
- [29] W. Rocchia, S. Sridharan, A. Nicholls, E. Alexov, A. Chiabrera, and B. Honig. Rapid grid-based construction of the molecular surface and the use of induced surface charge to calculate reaction field energies: Applications to the molecular systems and geometric objects. *Journal of Computational Chemistry*, 23:128–137, 2002.
- [30] S. N. Yu, Y. C. Zhou, and G. W. Wei. Matched interface and boundary (MIB) method for elliptic problems with sharp-edged interfaces. *Journal of Computational Physics*, 224(2):729–756, 2007.
- [31] S. N. Yu, W. H. Geng, and G. W. Wei. Treatment of geometric singularities in implicit solvent models. *Journal of Chemical Physics*, 126(24):244108, 2007.

- [32] T. J. You and S. C. Harvey. Finite-element approach to the electrostatics of macromolecules with arbitrary geometries. *Journal of Computational Chemistry*, 14:484–501, 1993.
- [33] C. M. Cortis and R. A. Friesner. Numerical simulation of the Poisson–Boltzmann equation using tetrahedral finite-element meshes. *Journal of Computational Chemistry*, 18(13):1591–1608, 1997.
- [34] P. B. Shaw. Theory of the Poisson Green’s-function for discontinuous dielectric media with an application to protein biophysics. *Physical Review A*, 32(4):2476–2487, 1985.
- [35] R. J. Zauhar and R. S. Morgan. A new method for computing the macromolecular electric-potential. *Journal of Molecular Biology*, 186(4):815–820, 1985.
- [36] R. J. Zauhar and R. S. Morgan. The rigorous computation of the molecular electric potential. *Journal of Computational Chemistry*, 9(2):171–187, 1988.
- [37] R. J. Zauhar and R. S. Morgan. Computing the electric-potential of biomolecules: application of a new method of molecular-surface triangulation. *Journal of Computational Chemistry*, 11(5):603–622, 1990.
- [38] R. J. Zauhar. SMART: A solvent-accessible triangulated surface generator for molecular graphics and boundary-element applications. *Journal of Computer-Aided Molecular Design*, 9(2):149–159, 1995.
- [39] B. J. Yoon and A. M. Lenhoff. A boundary element method for molecular electrostatics with electrolyte effects. *Journal of Computational Chemistry*, 11(9):1080–1086, 1990.
- [40] A. H. Juffer, E. F. F. Botta, B. A. M. van Keulen, A. van der Ploeg, and H. J. C. Berendsen. The electric potential of a macromolecule in a solvent: A fundamental approach. *Journal of Computational Physics*, 97(1):144–171, 1991.
- [41] H. X. Zhou. Boundary-element solution of macromolecular electrostatics - interaction energy between 2 proteins. *Biophysical Journal*, 65:955–963, 1993.
- [42] E. O. Purisima and S. H. Nilar. A simple yet accurate boundary-element method for continuum dielectric calculations. *Journal of Computational Chemistry*, 16(6):681–689, 1995.
- [43] E. O. Purisima. Fast summation boundary element method for calculating solvation free energies of macromolecules. *Journal of Computational Chemistry*, 19(13):1494–1504, 1998.
- [44] Y. N. Vorobjev and H. A. Scheraga. A fast adaptive multigrid boundary element method for macromolecular electrostatic computations in a solvent. *Journal of Computational Chemistry*, 18(4):569–583, 1997.

- [45] J. Liang and S. Subramaniam. Computation of molecular electrostatics with boundary element methods. *Biophysical Journal*, 73(4):1830–1841, 1997.
- [46] E. Cancès, B. Mennucci, and J. Tomasi. A new integral equation formalism for the polarizable continuum model: Theoretical background and applications to isotropic and anisotropic dielectrics. *Journal of Chemical Physics*, 107(8):3032–3041, 1997.
- [47] R. Bharadwaj, A. Windemuth, S. Sridharan, B. Honig, and A. Nicholls. The fast multipole boundary element method for molecular electrostatics: An optimal approach for large systems. *Journal of Computational Chemistry*, 16(7):898–913, 1995.
- [48] A. H. Boschitsch, M. O. Fenley, and W. K. Olson. A fast adaptive multipole algorithm for calculating screened Coulomb (Yukawa) interactions. *Journal of Computational Physics*, 151:212–241, 1999.
- [49] A. H. Boschitsch, M. O. Fenley, and H.-X. Zhou. Fast boundary element method for the linear Poisson–Boltzmann equation. *Journal of Physical Chemistry B*, 106(10):2741–54, 2002.
- [50] A. J. Bordner and G. A. Huber. Boundary element solution of the linear Poisson–Boltzmann equation and a multipole method for the rapid calculation of forces on macromolecules in solution. *Journal of Computational Chemistry*, 24(3):353–367, 2003.
- [51] D. M. Chipman. Solution of the linearized Poisson–Boltzmann equation. *Journal of Chemical Physics*, 120(12):5566–5575, 2004.
- [52] J. Tomasi, B. Mennucci, and R. Cammi. Quantum mechanical continuum solvation models. *Chemical Reviews*, 105:2999–3093, 2005.
- [53] P. Attard. Variational formulation for the electrostatic potential in dielectric continua. *Journal of Chemical Physics*, 119:1365–1372, 2003.
- [54] B. Z. Lu, D. Q. Zhang, and J. A. McCammon. Computation of electrostatic forces between solvated molecules determined by the Poisson–Boltzmann equation using a boundary element method. *Journal of Chemical Physics*, 122, 2005.
- [55] B. Z. Lu, X. L. Cheng, J. Huang, and J. A. McCammon. Order N algorithm for computation of electrostatic interactions in biomolecular systems. *Proceedings of the National Academy of Sciences of the USA*, 103(51):19314–19319, 2006.
- [56] D. Beglov and B. Roux. Solvation of complex molecules in a polar liquid: an integral equation theory. *Journal of Chemical Physics*, 104(21):8678–8689, 1996.
- [57] C. M. Stultz. An assessment of potential of mean force calculations with implicit solvent

- models. *Journal of Physical Chemistry B*, 108:16525–16532, 2004.
- [58] A. S. Thomas and A. H. Elcock. Direct observation of salt effects on molecular interactions through explicit-solvent molecular dynamics simulations: Differential effects on electrostatic and hydrophobic interactions and comparisons to Poisson–Boltzmann theory. *Journal of the American Chemical Society*, 128:7796–7806, 2006.
- [59] R. Penfold, B. Jönsson, and S. Nordholm. Ion-ion correlations in polyelectrolyte solutions: hard sphere counterions. *Journal of Chemical Physics*, 99:497–514, 1993.
- [60] T. Nishio and A. Minakata. Effects of ion size and valence on ion distribution in mixed counterion systems of rodlike polyelectrolyte solution. I. Mixed-size counterion systems with same valence. *Journal of Chemical Physics*, 113(23):10784–10792, 2000.
- [61] Z.-J. Tan and S.-J. Chen. Nucleic acid helix stability: effects of salt concentration, cation valence and size, and chain length. *Biophysical Journal*, 90:1175–1190, 2006.
- [62] S. Hofinger and T. Simonson. Dielectric relaxation in proteins: A continuum electrostatics model incorporating dielectric heterogeneity of the protein and time-dependent charges. *Journal of Computational Chemistry*, 22:290–305, 2001.
- [63] J. Tomasi and M. Persico. Molecular interactions in solution: An overview of methods based on continuous descriptions of the solvent. *Chemical Reviews*, 94:2027–2094, 1994.
- [64] J. P. Bardhan, M. D. Altman, J. K. White, and B. Tidor. Numerical integration techniques for curved-panel discretizations of molecule–solvent interfaces. *Journal of Chemical Physics*, 127:014701, 2007.
- [65] D. N. Chipman. Comparison of solvent reaction field representations. *Theoretical Chemistry Accounts*, 107(2):80–89, 2002.
- [66] M. Cossi, V. Barone, R. Cammi, and J. Tomasi. Ab initio study of solvated molecules: a new implementation of the polarizable continuum model. *Chemical Physics Letters*, 255(4-6):327–335, 1996.
- [67] R. Cammi and J. Tomasi. Remarks on the apparent-surface charges (ASC) methods in solvation problems: Iterative versus matrix-inversion procedures and the renormalization of the apparent charges. *Journal of Computational Chemistry*, 16(12):1449–1458, 1995.
- [68] R. J. Zauhar and A. Varnek. A fast and space-efficient boundary element method for computing electrostatic and hydration effects in large molecules. *Journal of Computational Chemistry*, 17:864–877, 1996.

- [69] K. E. Atkinson. *The Numerical Solution of Integral Equations of the Second Kind*. Cambridge University Press, 1997.
- [70] J. Tausch, J. Wang, and J. White. Improved integral formulations for fast 3-D method-of-moment solvers. *IEEE Transactions on Computer-Aided Design of Integrated Circuits and Systems*, 20(12):1398–1405, 2001.
- [71] M. D. Altman, J. P. Bardhan, J. K. White, and B. Tidor. An efficient and accurate surface formulation for biomolecule electrostatics in non-ionic solution. In *Engineering in Medicine and Biology Conference (EMBC)*, 2005.
- [72] D. Sitkoff, K. A. Sharp, and B. Honig. Accurate calculation of hydration free energies using macroscopic solvent models. *Journal of Physical Chemistry B*, 98:1978–1988, 1994.
- [73] M. Nina, W. Im, and B. Roux. Optimized atomic radii for protein continuum electrostatics solvation forces. *Biophysical Chemistry*, 78:89–96, 1999.
- [74] B. Lee and F. M. Richards. The interpretation of protein structures: Estimation of static accessibility. *Journal of Molecular Biology*, 55(3):379–400, 1971.
- [75] F. M. Richards. Areas, volumes, packing, and protein structure. *Annual Review of Biophysics and Bioengineering*, 6:151–176, 1977.
- [76] M. L. Connolly. Analytical molecular surface calculation. *Journal of Applied Crystallography*, 16:548–558, 1983.
- [77] J. B. Foresman, T. A. Keith, K. B. Wiberg, J. Snoonian, and M. J. Frisch. Solvent effects. 5. Influence of cavity shape, truncation of electrostatics, and electron correlation on ab initio reaction field calculations. *Journal of Physical Chemistry*, 100:16098, 1996.
- [78] C.-G. Zhan, J. Bentley, and D. M. Chipman. Volume polarization in reaction field theory. *Journal of Chemical Physics*, 108:177, 1998.
- [79] T. Simonson. Macromolecular electrostatics: Continuum models and their growing pains. *Current Opinions in Structural Biology*, 11:243–252, 2001.
- [80] C. N. Schutz and A. Warshel. What are the dielectric constants of proteins and how to validate electrostatic models? *Proteins: Structure, Function, Genetics*, 44:400–417, 2001.
- [81] J. D. Jackson. *Classical Electrodynamics*. Wiley, 3rd edition, 1998.
- [82] M. D. Altman, J. P. Bardhan, J. K. White, and B. Tidor. Accurate solution of multi-region continuum electrostatic problems using the linearized Poisson–Boltzmann equation and curved boundary elements. (*in review, Journal of Computational Chemistry*).

- [83] J. O'M Bockris and A. K. N. Reddy. *Modern Electrochemistry: An Introduction to an interdisciplinary area*. Plenum Press, 1973.
- [84] C. Pozrikidis. *A Practical Guide to Boundary-Element Methods with the Software Library BEMLIB*. Chapman & Hall/CRC Press, 2002.
- [85] J. Nedelec. Curved finite element methods for the solution of singular integral equations on surfaces in \mathbb{R}^3 . *Computer Methods in Applied Mechanics and Engineering*, 8:61–80, 1976.
- [86] B. Buchmann. Accuracy and stability of a set of free-surface time-domain boundary element models based on B-splines. *International Journal for Numerical Methods in Fluids*, 33(1):125–155, 2000.
- [87] M. H. Lean and A. Wexler. Accurate numerical-integration of singular boundary element kernels over boundaries with curvature. *International Journal For Numerical Methods in Engineering*, 21(2):211–228, 1985.
- [88] A. E. Ruehli and P. A. Brennan. Efficient capacitance calculations for three-dimensional multiconductor systems. *IEEE Transactions on Microwave Theory and Techniques*, 21:76–82, 1973.
- [89] A. Stroud. *Approximate Calculation of Multiple Integrals*. Prentice Hall, 1971.
- [90] J. L. Hess and A. M. O. Smith. Calculation of non-lifting potential flow about arbitrary three-dimensional bodies. *Journal of Ship Research*, 8(2):22–44, 1962.
- [91] J. N. Newman. Distribution of sources and normal dipoles over a quadrilateral panel. *Journal of Engineering Mathematics*, 20(2):113–126, 1986.
- [92] M. Sanner, A. J. Olson, and J. C. Spehner. Reduced surface: An efficient way to compute molecular surfaces. *Biopolymers*, 38:305–320, 1996.
- [93] M. D. Altman, J. P. Bardhan, B. Tidor, and J. K. White. FFTSVD: A fast multiscale boundary-element method solver suitable for BioMEMS and biomolecule simulation. *IEEE Transactions on Computer-Aided Design of Integrated Circuits and Systems*, 25(2):274–284, 2006.
- [94] K. Nabors and J. White. FASTCAP: A multipole accelerated 3-D capacitance extraction program. *IEEE Transactions on Computer-Aided Design of Integrated Circuits and Systems*, 10(10):1447–1459, 1991.
- [95] L. Greengard. *The Rapid Evaluation of Potential Fields in Particle Systems*. MIT Press, 1988.

- [96] J. R. Phillips and J. K. White. A precorrected-FFT method for electrostatic analysis of complicated 3-D structures. *IEEE Transactions on Computer-Aided Design of Integrated Circuits and Systems*, 16(10):1059–1072, 1997.
- [97] Z. Zhu, B. Song, and J. White. Algorithms in FastImp: A fast and wideband impedance extraction program for complicated 3D geometries. *IEEE/ACM Design Automation Conference (DAC)*, 2003.
- [98] Y. Saad and M. Schultz. GMRES: A generalized minimal residual algorithm for solving nonsymmetric linear systems. *SIAM Journal of Scientific and Statistical Computing*, 7:856–869, 1986.
- [99] S. S. Kuo, M. D. Altman, J. P. Bardhan, B. Tidor, and J. K. White. Fast methods for simulation of biomolecule electrostatics. In *International Conference on Computer Aided Design (ICCAD)*, 2002.
- [100] P. Lavigne, M. P. Crump, S. M. Gagné, R. S. Hodges, C. M. Kay, and B. D. Sykes. Insights into the mechanism of heterodimerization from the 1H-NMR solution structure of the c-Myc-Max heterodimeric leucine zipper. *Journal of Molecular Biology*, 281(1):165–181, 1998.
- [101] M. Feig and C. L. Brooks III. Recent advances in the development and application of implicit solvent models in biomolecule simulations. *Curr. Opin. Struct. Bio.*, 14:217–224, 2004.

Figures:

- 1 A continuum-solvent model for molecular electrostatics
- 2 Absolute error between analytical solution and numerical solutions of the ASC formulation and the simplified-Juffer formulation, for a 1 Å-radius sphere with central +1 e charge in non-ionic solution. The notation in the legend is as follows: ASC, apparent-surface-charge-formulation; SJ, simplified-Juffer formulation; t, test-inner discretization; b, basis-inner discretization; the final number is the order of the quadrature rule n_p used to evaluate the outer integrals.
- 3 Simulations of the unit sphere with centrally located unit charge performed using the Bordner–Huber and Yoon–Lenhoff formulations in non-ionic solvent. (a) and (b) Absolute deviations between the analytical electrostatic free energy and numerical solutions of the YL and BH formulations, using different discretization methods and as a function of the number of boundary elements, for a 1 Å-radius sphere with central +1 e charge in non-ionic solution. Notation in the legend is as in Figure 2. (c) Absolute deviation of calculated electrostatic free energies from reference calculations employing 18-point quadrature rules. Basis-inner discretizations are compared to an 18-point basis-inner method and 18-point test-inner calculations are used as a reference for the test-inner calculations.
- 4 Convergence of calculated answers towards a high-resolution reference simulation of formamide. (a) The ASC formulation. (b) The J formulation. (c) The YL formulation.
- 5 Convergence of GMRES [98] when simulating formamide using the ASC/SJ, BH/YL, and J formulations, with and without preconditioning, and using either 1-point basis-inner or test-inner Galerkin approximations. (a) Convergence of the SJ formulation. (b) Convergence of the YL formulation. (c) Convergence of the J formulation.
- 6 Deviation of electrostatic free energies relative to a reference calculation, discretizing the Galerkin double integrals in a kernel-dependent manner. Basis-inner discretizations are used for all entries associated with single-layer and

dipole-induced electric-field operators. (a) The J formulation discretized using basis-inner methods only or with the normal-electric-field operator discretized using test-inner methods. Results are plotted as deviations from a high-accuracy curved-element simulation. (b) The J formulation with the dipole-layer and the normal-electric-field operators, or the dipole-layer operator only, discretized using test-inner methods. Results are plotted as deviations from a high-accuracy curved-element simulation. (c) The YL formulation discretized using basis-inner or test-inner methods for the double-layer potential. Results are plotted as deviations from a calculation employing 18-point quadrature.

7 Deviations of calculated electrostatic free energies for a 32-residue α -helix [100, 101], relative to a high-resolution reference calculation. (a) The ASC formulation. (b) The YL formulation. (c) The J formulation.

NOTICE

The submitted manuscript has been created by the University of Chicago, LLC as Operator of Argonne National Laboratory (“Argonne”). Argonne, a U.S. Department of Energy Office of Science laboratory, is operated under Contract No. DE-AC02-06CH11357. The U.S. Government retains for itself, and others acting on its behalf, a paid-up, nonexclusive, irrevocable worldwide license in said article to reproduce, prepare derivative works, distribute copies to the public, and perform publicly and display publicly, by or on behalf of the Government.

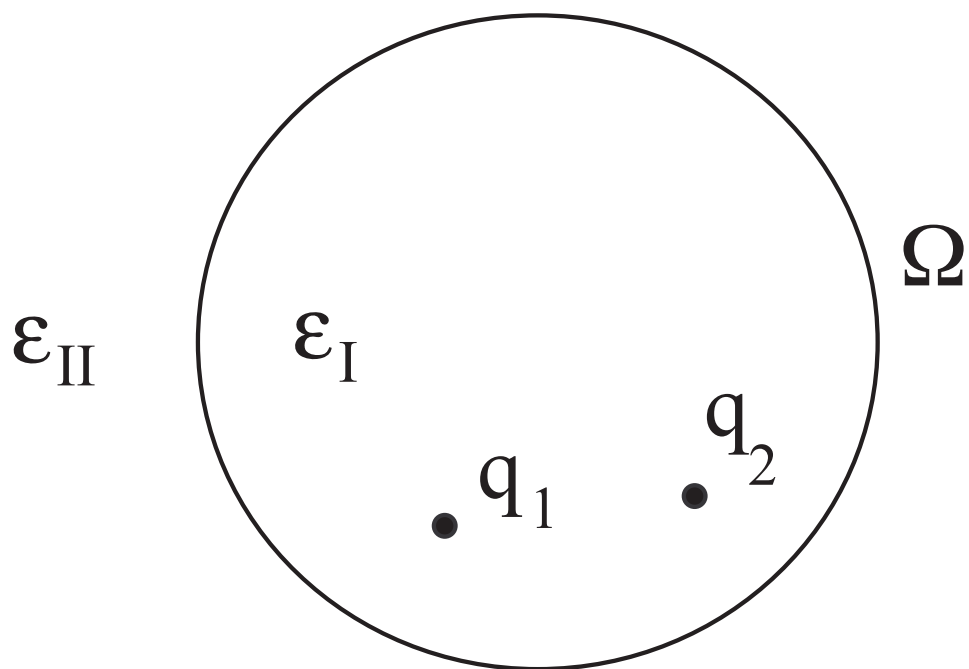


FIG. 1: A continuum-solvent model for molecular electrostatics.

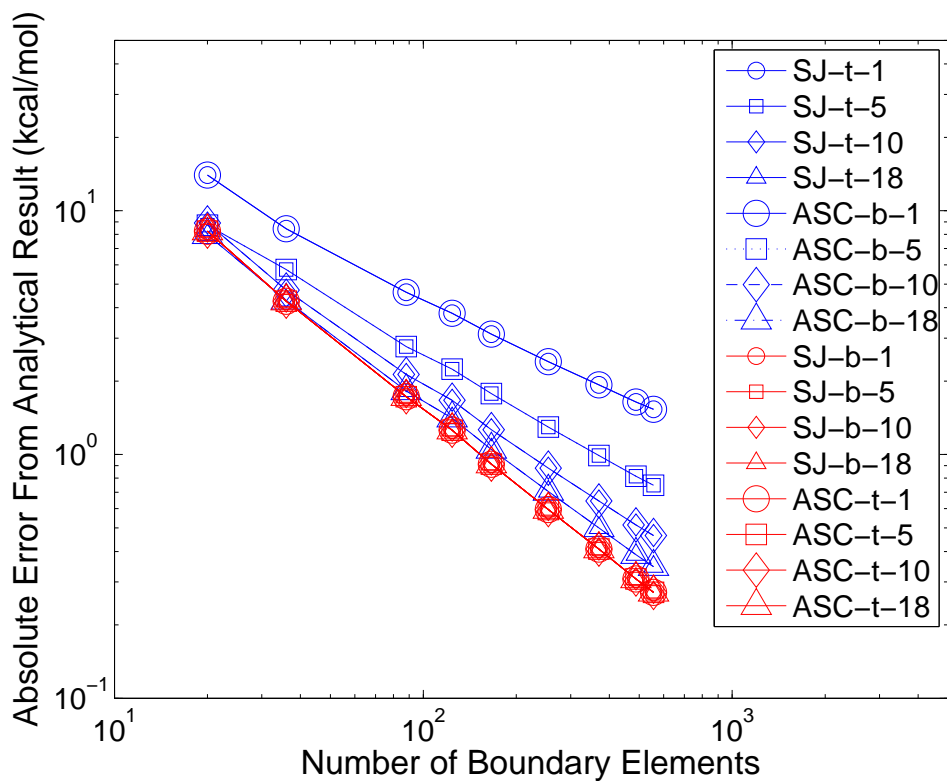


FIG. 2: Absolute error between analytical solution and numerical solutions of the ASC formulation and the simplified-Juffer formulation, for a 1 Å-radius sphere with central +1 e charge in non-ionic solution. The notation in the legend is as follows: ASC, apparent-surface-charge-formulation; SJ, simplified-Juffer formulation; t, test-inner discretization; b, basis-inner discretization; the final number is the order of the quadrature rule n_p used to evaluate the outer integrals.

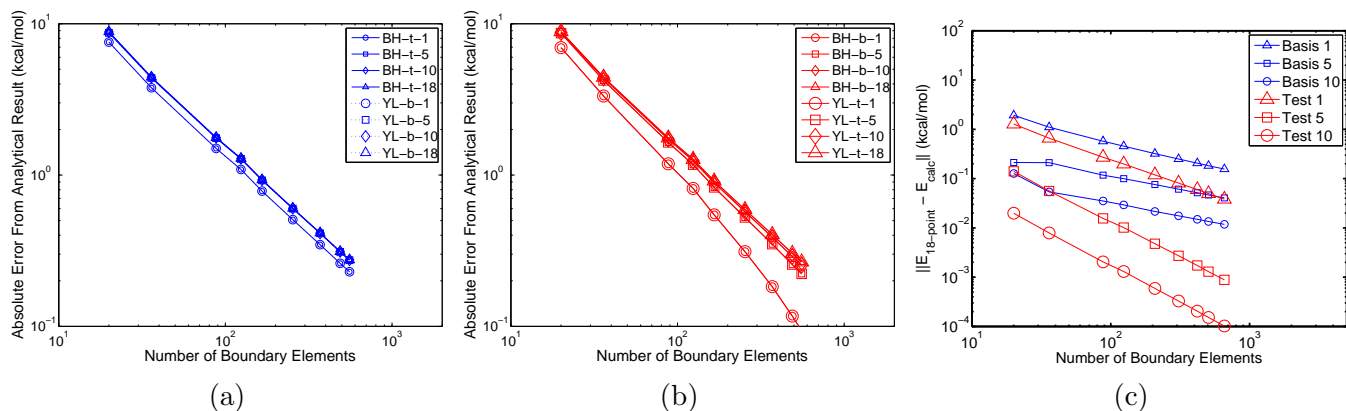


FIG. 3: Simulations of the unit sphere with centrally located unit charge performed using the Bordner–Huber and Yoon–Lenhoff formulations in non-ionic solvent. (a) and (b) Absolute deviations between the analytical electrostatic free energy and numerical solutions of the YL and BH formulations, using different discretization methods and as a function of the number of boundary elements, for a 1 Å-radius sphere with central +1 e charge in non-ionic solution. Notation in the legend is as in Figure 2. (c) Absolute deviation of calculated electrostatic free energies from reference calculations employing 18-point quadrature rules. Basis-inner discretizations are compared to an 18-point basis-inner method and 18-point test-inner calculations are used as a reference for the test-inner calculations.

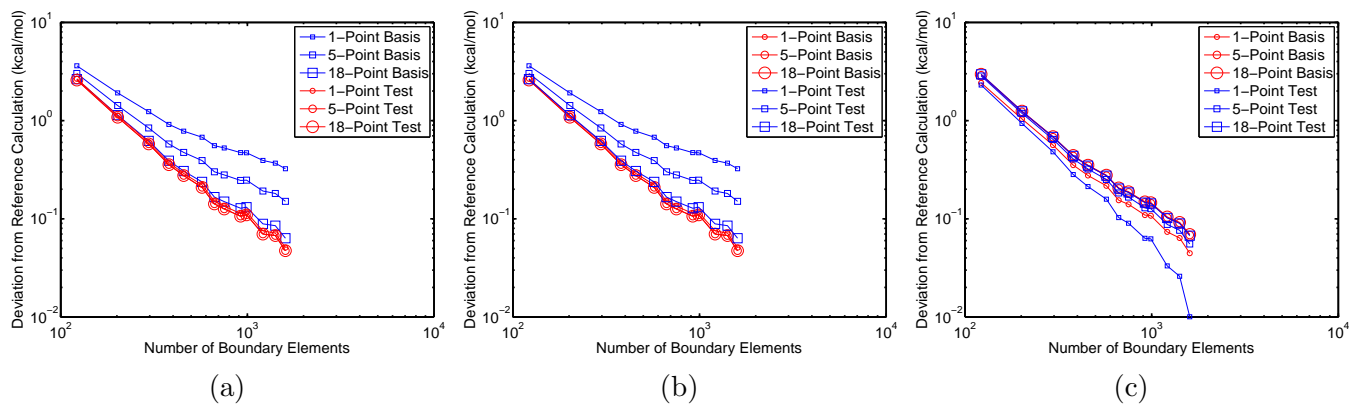


FIG. 4: Convergence of calculated answers towards a high-resolution reference simulation of formamide. (a) The ASC formulation. (b) The J formulation. (c) The YL formulation.

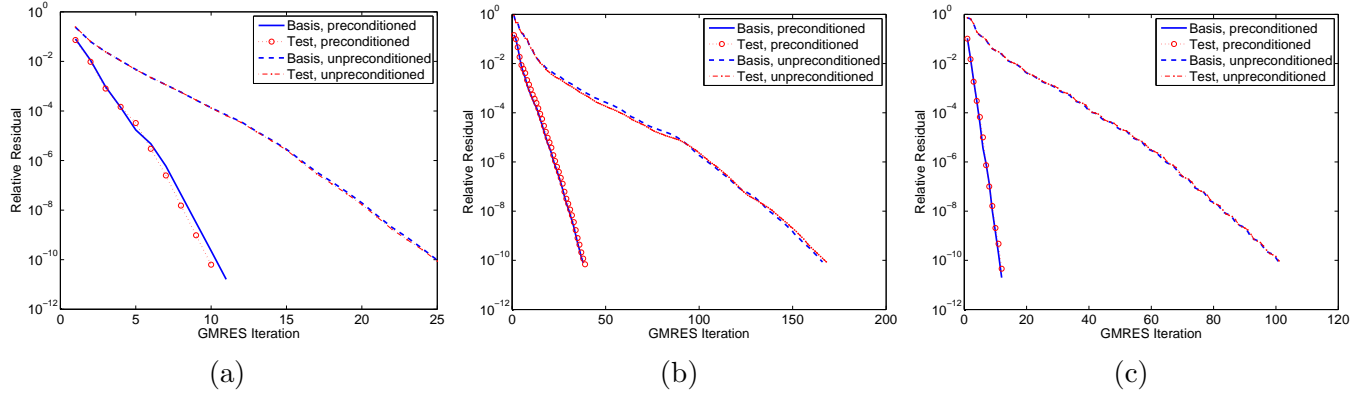


FIG. 5: Convergence of GMRES [98] when simulating formamide using the ASC/SJ, BH/YL, and J formulations, with and without preconditioning, and using either 1-point basis-inner or test-inner Galerkin approximations. (a) Convergence of the SJ formulation. (b) Convergence of the YL formulation. (c) Convergence of the J formulation.

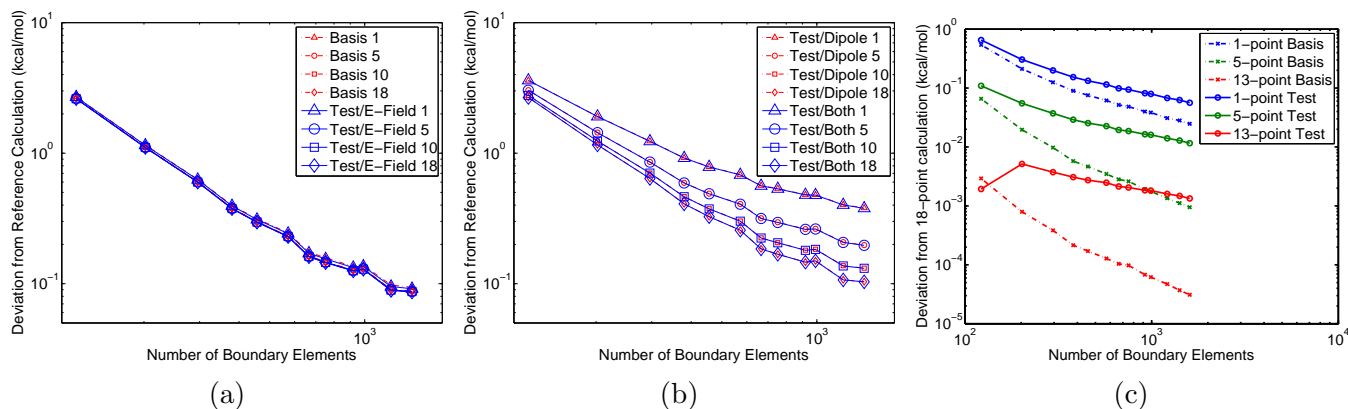


FIG. 6: Deviation of electrostatic free energies relative to a reference calculation, discretizing the Galerkin double integrals in a kernel-dependent manner. Basis-inner discretizations are used for all entries associated with single-layer and dipole-induced electric-field operators. (a) The J formulation discretized using basis-inner methods only or with the normal-electric-field operator discretized using test-inner methods. Results are plotted as deviations from a high-accuracy curved-element simulation. (b) The J formulation with the dipole-layer and the normal-electric-field operators, or the dipole-layer operator only, discretized using test-inner methods. Results are plotted as deviations from a high-accuracy curved-element simulation. (c) The YL formulation discretized using basis-inner or test-inner methods for the double-layer potential. Results are plotted as deviations from a calculation employing 18-point quadrature.

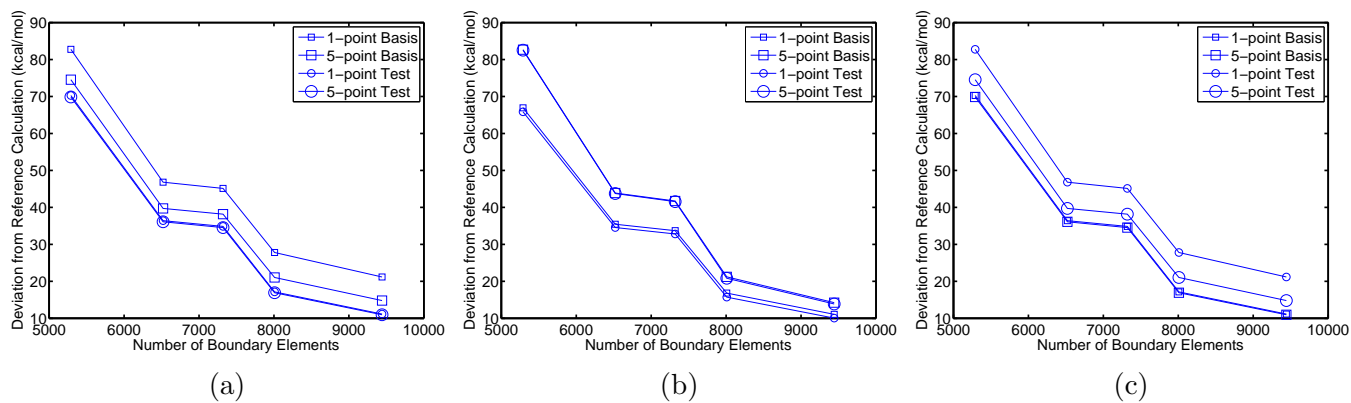


FIG. 7: Deviations of calculated electrostatic free energies for a 32-residue α -helix [100, 101], relative to a high-resolution reference calculation. (a) The ASC formulation. (b) The YL formulation. (c) The J formulation.